JOURNAL OF GUIDANCE, CONTROL, AND DYNAMICS
Vol. 26, No. 2, March–April 2003

Escaping Trajectories in the Hill Three-Body Problem and Applications

B. F. Villac* and D. J. Scheeres†
University of Michigan, Ann Arbor, Michigan 48109-2140

Low-energy escaping trajectories in the Hill three-body problem are investigated numerically using a Poincaré map that relates the crossing of a plane containing one of the collinear libration points back to the first periapsis passage. This set of periapsis points is confined in a small region that determines some conditions for escape from any planetary satellite. In particular, the minimum energy to escape from a given circular orbit is obtained together with restrictions on the initial conditions (inclination, argument of periapsis, and longitude of the ascending node). This leads to a new optimal transfer criterion for the class of directly escaping trajectories. Savings on the order of 130 m/s in the case of Europa are obtained when compared to a classic two-body model. The results are also extended to the problem of low-energy capture. Numerical applications are given for the cases of Miranda, Europa, Titan, and Triton.

Introduction

LOW-ENERGY transit trajectories have been investigated by several authors, all pointing out the possibility of obtaining large savings in fuel cost (as compared to classical approaches) by using the natural dynamics arising from the presence of a third (or fourth) body. Conley[1] gave the first analysis of the structure of the flow near the colinear libration points in the planar circular restricted three-body problem (PCR3BP). He proved the existence of transit trajectories going from a region dominated by the gravitational attraction of the primary to a region dominated by the secondary (Hill's regions). From the viewpoint of the primary, these trajectories correspond to escaping trajectories. Belbruno[2] pointed out that these nonlinear dynamics can be used to numerically compute ballistic transfers to the moon and gave several ways of finding such transfers. More recent work by Koon et al.[3,4] gives a more rigorous explanation of these phenomena by applying some techniques from dynamical systems theory to systems of coupled PCR3BP. They obtained a systematic way of designing ballistic lunar transfers and, more generally, trajectories with a predetermined future and past (in terms of transfer from one Hill's region to another). In this paper we give another view of the geometry of escaping trajectories, focusing on obtaining practical characterizations of the trajectories. Sharp estimates on the initial conditions of these escaping trajectories at periapsis are obtained, and applications of these results are made to the analysis of direct escape maneuvers. In particular, the minimum energy needed to directly escape, starting at a given altitude, are obtained. These results should be useful for mission design and planning.

This study was motivated by the Europa Orbiter mission, where the end-of-mission disposal of the spacecraft is an issue for planetary protection, and escape from Europa at the end of the mission has been investigated as one possible solution. Hence, estimates of the cost for direct escape are obtained, although we do not address the long-term behavior of these escape trajectories, which constitutes another aspect of the disposal problem. Also, by the nature of our motivating problem this paper is focused on the case of planetary satellite orbiters, even though the results obtained are of wider application because the Hill model used for this analysis also gives a good description of the dynamics of planetary orbiters, coorbital satellites, or, more generally, of two close masses in the gravitational attraction of a larger one.[5]

We know from classical results on the Hill problem[6] that escape is only possible when the zero velocity surface opens at the colinear libration points L_1 and L_2, setting up a minimal value of the Jacobi integral for escape. Escaping trajectories must then cross a plane containing L_1 or L_2 with a positive outward velocity. This condition is not equivalent to escape because the spacecraft can be "caught" temporarily on the stable manifold of a Lyapunov orbit about L_1 or L_2. However, an arbitrary small ΔV can push the spacecraft onto the unstable manifold departing from L_1 or L_2. Thus, in the following, escaping trajectories will mean trajectories having a positive outward velocity at the crossing of a plane containing L_1 or L_2. In this setting practical engineering characterizations of escape that can be useful in mission design can be obtained. As a consequence, the analysis is focused on the dynamics close to the primary, which justifies the use of the Hill three-body problem (H3BP) as the underlying model. Moreover, the assumptions of this model are met for most planetary satellites of interest in the solar system, making this model well suited for the investigation of a range of practical applications.[7]

The characterizations obtained are computed by using a Poincaré map that relates the crossing of the escaping trajectories through a plane containing L_2 with the previous periapsis radius vector of those trajectories. This computation is made for constant values of the Jacobi energy (just above the critical value), allowing us to reduce the dimensionality of the system. The resulting set of periapsis points that lead to escape is confined to a small region, symmetric about the equatorial plane, which can be used to determine the minimum energy required and constraints on the initial conditions to escape from the satellite. Moreover, by using the symmetry properties of the Hill model, these computations can be transformed to characterize the first periapsis of low-energy capture trajectories.

Applications of the preceding results are then made to the problem of directly escaping trajectories assuming a spacecraft initially in a low-altitude, circular orbit. Hénon[8] showed, indeed, that quasi-circular, stable, periodic orbits exist in the planar H3BP, and for nonzero inclination Scheeres et al.[7] showed that below and above a critical inclination ($\simeq$45 and 135 deg, respectively) low circular orbits are stable about most planetary satellites in the solar system. These orbits have small quasi-periodic variations in eccentricity that can be neglected at first approximation in the case of low-altitude trajectories. Therefore, in order to characterize the cost of escape maneuvers we assume that, at low altitudes, a spacecraft is in a Keplerian circular orbit and investigate how much ΔV is needed for this spacecraft to escape from such a circular orbit.

In this paper we show that the minimum ΔV to escape directly is obtained for tangential burns and that this minimum decreases

Received 25 March 2002; revision received 1 October 2002; accepted for publication 8 October 2002.

*Ph.D. Candidate, Department of Aerospace Engineering; bvillac@umich.edu. Student Member AIAA.

†Associate Professor, Department of Aerospace Engineering; scheeres@umich.edu. Senior Member AIAA.

as altitude increases. A new optimality criterion is then stated for the class of directly escaping trajectories using one impulsive maneuver, resulting in fuel savings on the order of 130 m/s in the case of Europa (as compared to a two-body Keplerian model). Given an initial altitude, the optimal Jacobi constant and the minimum ΔV required to reach escape can be read from some graphs. The time of the maneuver is determined by a condition on the longitude of the ascending node and the argument of periapsis of the transfer trajectory. Restrictions on the inclination for these transfers to be possible also exist, as the initial orbit must be near equatorial. A simple scaling of these results allows us to map our analysis to any planetary satellite (assuming the Hill model), as given in the Appendix.

Hill Three-Body Dynamics

The circular restricted three-body problem (CR3BP) describes the dynamics of a massless object attracted by two point masses revolving around each other in a circular orbit. This model has found many applications in both astronomy and astrodynamics; indeed, it is the simplest model of the main perturbation of an object in interplanetary space (e.g., comet, Jupiter, sun system) or even for Earth orbiters for high enough altitude.[9] In particular, this model gives a good description of the dynamics around a planetary satellite. However, in this case when the dynamics close to the smaller primary are considered the Hill three-body model viewed as a limiting case of the CR3BP also gives a good description of the dynamics and consists of a simpler set of equations (without any free parameters). The Hill model has, however, a much wider generality because it also covers the dynamics of two small masses in a circular orbit about a larger one. In particular, the Hill model gives a good description of the dynamics of coorbital satellites and can be used to describe the dynamics in planetary rings or the accretion properties of planets in formation.[5] In this first section a brief account of the basic properties of the Hill's problem used in the subsequent analysis is given.

Equations of Motion

The Hill model can be obtained from the CR3BP by taking the center of the coordinate system to be at the center of the primary (smaller body, planetary satellite for example) and letting the mass ratio of the primary to the secondary go to zero while scaling the coordinates to remain finite.[10] The resulting equations of motion can be written as

$$\ddot{x} - 2N\dot{y} = -(\mu/r^3)x + 3N^2x \tag{1}$$

$$\ddot{y} + 2N\dot{x} = -(\mu/r^3)y \tag{2}$$

$$\ddot{z} = -(\mu/r^3)z - N^2z \tag{3}$$

where N is the angular velocity of the motion of the primary around the secondary, μ is the gravitational parameter of the primary, and $r = \sqrt{(x^2 + y^2 + z^2)}$ is the magnitude of the position vector (see Fig. 1). Note that for $N = 0$ rad/s the preceding equations reduce to the classical two-body problem.

We immediately see that the solutions $x = \pm(\mu/3N^2)^{1/3}$, $y = z = \dot{x} = \dot{y} = \dot{z} = 0$ are particular solutions of these equations. They correspond to the analog of the libration points L_1 and L_2 in the CR3BP, but are now symmetric about the origin. (L_1 has a negative abscissa and L_2 has a positive one; see Fig. 2.)

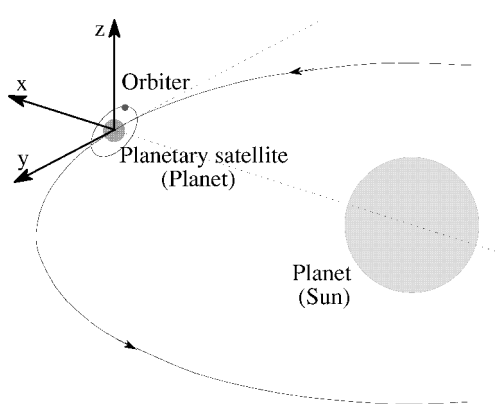

Fig. 1 Geometry of the Hill problem in the case of an orbiter.

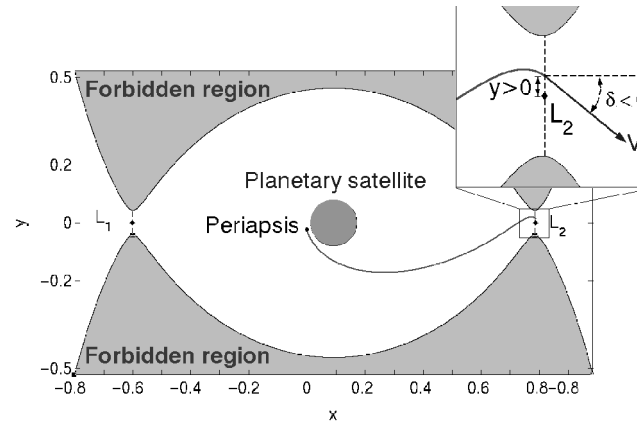

Fig. 2 Geometry of the Poincaré map.

Zero Velocity Surfaces and Escape

Similar to the CR3BP, the Hill model has a nontrivial integral of motion, the Jacobi constant J:

$$J = \tfrac{1}{2}v^2 - \mu/r - \tfrac{1}{2}N^2(3x^2 - z^2) \tag{4}$$

where $v = \sqrt{(\dot{x}^2 + \dot{y}^2 + \dot{z}^2)}$ is the speed of the particle. This constant has deep consequences for the dynamics of the motion. In particular, the physical condition $v^2 \geq 0$ in Eq. (4) imposes a restriction on the allowable position space for the motion at any given value of J. Setting $v = 0$, Eq. (4) gives the implicit definition of a surface upon which the velocity is zero, thus delimiting the physical boundary of allowable motion (see Fig. 2).

In our case it also gives a minimum threshold that must be reached for escape to occur. More precisely, escape becomes possible for $J > J_{L_{1,2}}$ where

$$J_{L_{1,2}} = -\tfrac{1}{2}(9\mu N)^{\frac{2}{3}} \tag{5}$$

This corresponds to the critical value of J for which the zero velocity surfaces open at L_1 and L_2. As explained in the Introduction, escaping trajectories correspond, in this paper, to trajectories that cross either plane $x = x_{L_{1,2}}$ in the outward direction. We will analyze some characteristics of these trajectories with a Jacobi constant just above the critical value of $J_{L_{1,2}}$, corresponding to the lowest energy possible for escaping trajectories.

Symmetries and Extension to the Capture Problem

As a limiting case of the CR3BP, the Hill model takes advantage of "almost symmetries" present in the CR3BP by turning them into exact mathematical symmetries. For example, the points L_1 and L_2 are now symmetric about the origin.

More precisely, if $(x, y, z, \dot{x}, \dot{y}, \dot{z}, t)$ denotes a solution of the equations of motion then the trajectories obtained by applying the following transformations are also valid solutions:

$$(x, y, z, \dot{x}, \dot{y}, \dot{z}, t) \xrightarrow{S_1} (-x, y, z, \dot{x}, -\dot{y}, -\dot{z}, -t) \tag{6}$$

$$(x, y, z, \dot{x}, \dot{y}, \dot{z}, t) \xrightarrow{S_2} (x, -y, z, -\dot{x}, \dot{y}, -\dot{z}, -t) \tag{7}$$

$$(x, y, z, \dot{x}, \dot{y}, \dot{z}, t) \xrightarrow{S_3} (x, y, -z, \dot{x}, \dot{y}, -\dot{z}, t) \tag{8}$$

The composition of these three symmetries yield other symmetries, notably the composition of Eqs. (1), (2) and (1), (2), (3) yield

$$(x, y, z, \dot{x}, \dot{y}, \dot{z}, t) \xrightarrow{S_4} (-x, -y, z, -\dot{x}, -\dot{y}, \dot{z}, t) \tag{9}$$

$$(x, y, z, \dot{x}, \dot{y}, \dot{z}, t) \xrightarrow{S_5} (-x, -y, -z, -\dot{x}, -\dot{y}, -\dot{z}, t) \tag{10}$$

This last symmetry is a pure symmetry about the origin, which results in the symmetry of L_1 and L_2. Also from S_5 we see that if $\mathcal{X} = (x, y, z, \dot{x}, \dot{y}, \dot{z}, t)$ is an escaping trajectory about L_2, then

Table 1 Length and timescales of the solar system planetary satellites

Planet		Satellite	μ, km^3/s^2	N, 1/s	l, km	τ, hr	Radius, km	Normalized radius	Type
Earth		Moon	4.903E+03	2.662E−06	88,454.7	104.36	1,738	0.0196	2
Mars	I	Phobos	6.4E−04	2.280E−04	23.1	1.22	11	0.4859	1
	II	Deimos	1.3E−04	5.760E−05	33.8	4.82	6	0.1881	1
Jupiter	I	Io	5.930E+03	4.111E−05	15,196.3	6.76	1,815	0.1194	1
	II	Europa	3.193E+03	2.048E−05	19,672.6	13.56	1,569	0.0797	2
	III	Ganymede	9.883E+03	1.016E−05	45,733.4	27.33	2,631	0.0575	2
	IV	Callisto	7.171E+03	4.357E−06	72,283.6	63.75	2,400	0.0332	2
	V	Amalthea	4.814E−01	1.460E−04	282.7	1.90	98	0.3454	1
	VI	Himalia	6.335E−01	2.902E−07	19,592.3	957.09	93	0.0047	2
	VII	Elara	5.068E−02	2.801E−07	8,645.0	991.80	38	0.0044	2
	VIII	Pasiphae	1.267E−02	9.894E−08	10,897.8	2,807.49	25	0.0023	2
	IX	Sinope	5.070E−03	9.594E−08	8,196.2	2,895.35	18	0.0022	2
	X	Lysithea	5.070E−03	2.805E−07	4,008.2	990.15	81	0.0202	2
	XI	Carme	6.330E−03	1.051E−07	8,308.9	2,643.25	20	0.0024	2
	XII	Ananke	2.530E−03	1.152E−07	5,756.7	2,410.24	15	0.0026	2
	XIII	Leda	3.800E−04	3.046E−07	1,600.0	911.84	8	0.0050	2
	XIV	Thebe	5.068E−02	1.078E−04	163.4	2.58	50	0.3060	1
	XV	Adrastea	1.270E−03	2.438E−04	27.7	1.14	10	0.3606	1
	XVI	Metis	6.330E−03	2.467E−04	47.0	1.13	20	0.4251	1
Saturn	I	Mimas	3.035E+00	7.717E−05	798.8	3.60	196	0.2453	1
	II	Enceladus	4.931E+00	5.307E−05	1,205.2	5.23	250	0.2074	1
	III	Thethys	4.931E+01	3.852E−05	3,215.0	7.21	530	0.1648	1
	IV	Dione	7.018E+01	2.657E−05	4,632.3	10.45	560	0.1208	1
	V	Rhea	1.669E+02	1.610E−05	8,636.0	17.26	765	0.0885	1
	VI	Titan	9.028E+03	4.561E−06	75,714.8	60.91	2,575	0.0340	2
	VII	Hyperion	1.138E+00	3.418E−06	4,601.2	81.27	148	0.0322	2
	VIII	Lapetus	1.252E+02	9.167E−07	53,010.4	303.02	730	0.0137	2
	IX	Phoebe	2.655E−02	1.321E−07	11,501.6	2,102.68	110	0.0095	2
Uranus	I	Ariel	9.017E+01	2.885E−05	4,766.7	9.63	579	0.1214	1
	II	Umbriel	7.803E+01	1.755E−05	6,328.1	15.83	586	0.0926	1
	III	Titania	2.347E+02	8.353E−06	14,982.5	33.25	790	0.0527	2
	IV	Oberon	2.006E+02	5.402E−06	19,014.2	51.43	762	0.0400	2
	V	Miranda	4.624E+00	5.145E−05	1,204.4	5.40	240	0.1992	1
Neptune	I	Triton	1.433E+03	1.237E−05	21,075.1	22.45	1,353	0.0642	2
	II	Nereid	1.372E+00	2.019E−07	32,280.8	1,375.62	170	0.0052	2
Pluto	I	Charon	2.202E+02	1.139E−05	11,931.7	24.40	593	0.0497	2

$S_5(\mathcal{X})$ is an escaping trajectory about L_1. In other words, if $P(\mathcal{X})$ is a property of an L_2 escaping trajectory, then $S_5[P(\mathcal{X})]$ will be the corresponding property of the L_1 escaping trajectory. Therefore, we have a 1:1 correspondance between L_1 and L_2, and we can restrict the analysis to L_2 escaping trajectories.

From S_3 we see that the same is true for reflections about the (x, y) plane, allowing us to restrict the analysis to escaping trajectories having a positive z coordinate. This is used to simplify the computation of the Poincaré maps.

The symmetries S_1 and S_2 involve a reflection in time, indicating that if $\mathcal{X}$ is an escaping trajectory, then $S_{1,2}(\mathcal{X})$ will be a capture trajectory. By this, we mean trajectories coming from the exterior region and crossing the planes $x = x_{L_{1,2}}$ with an inward velocity. These trajectories have at least one of their periapses in the Hill region, but are not necessarily captured for long periods of time. As some examples will show, these trajectories can directly impact the planetary satellite under consideration. Thus, applying S_1 or S_2 to escaping trajectories we immediately obtain a corresponding characterisation for capture trajectories.

Normalization and Scaling to Any Planetary Satellite

Besides these symmetry properties, the form of the Hill equations of motion allows for the nondimensionalization of the model and elimination of all free parameters. More precisely, by taking $l = (\mu/N^2)^{1/3}$ as the unit length and $\tau = 1/N$ as the unit time the equations of motion transform into the following parameterless equations:

$$\ddot{x} - 2\dot{y} = -x/r^3 + 3x \tag{11}$$

$$\ddot{y} + 2\dot{x} = -y/r^3 \tag{12}$$

$$\ddot{z} = -z/r^3 - z \tag{13}$$

From a formal point of view, all dimensional quantities are nondimensionalized by taking $N = 1$ and $\mu = 1$, so that in the nondimensional setting

$$J_{L_{1,2}} = -\tfrac{1}{2}(9)^{\frac{2}{3}} = -2.163\ldots \tag{14}$$

$$x_{L_{1,2}} = \pm\left(\tfrac{1}{3}\right)^{\frac{1}{3}} = \pm 0.693\ldots \tag{15}$$

All computations performed on Eqs. (11–13) can be directly scaled to any physical system modeled by the Hill equations by simply scaling the results. In particular, all of the analysis that follows applies to most planetary satellites of interest in the solar system.[7] Table 1 gives the length and timescale for most of the planetary satellites of the solar system, whose mass, orbital period, and radius are known.[11] (The last column of this table will be explained in subsection Results.)

In the remainder of this paper, computations will be performed in the nondimensional setting, with some scaled results being given in the Appendix. Note that these scalings depend both on the physical parameters of the primaries as well as their orbital characteristics (mean motion N). Therefore, planetary satellites of different mass and radius might have the same radius in nondimensionalized coordinates.

Poincaré Map

A Poincaré map generally refers to the association of a discrete time system given an initial, more complicated, continuous time dynamical system. It allows us to reduce the dimensionality of the system by at least one and by two if there exists a first integral, as is the case in the Hill model. Our use of a Poincaré map will be mostly numerical, giving us a convenient way to represent some properties of the flow and allowing us to numerically extract some constraints on initial conditions.

Although generally applied to periodic orbits or to study the structure of flows near homoclinic/heteroclinic trajectories,[12] the definition of a Poincaré map really requires only the choice of two surfaces of sections transversal to the flow in phase space and can be used in more general ways. The study of the Poincaré map is that of a discrete map from one surface of section to the next one.

In this section the Poincaré map used and the characterizations of the escaping trajectories obtained are described. These characterizations represent restrictions on the periapsis of a trajectory in order that it directly escapes (or be captured).

Computation of the Map

For our purpose we use a map relating escaping trajectories (i.e., having $\dot{x} > 0$ at $x = x_{L_2}$ near the equilibrium L_2) back to their first periapsis. The initial surface of section Σ_1 is hence the cross section of the plane $x = x_{L_2}$ with the Hill region and the image surface Σ_2 being the set defined by the periapsis condition $\dot{r} = 0$ and $\ddot{r} > 0$ prior to Σ_1. It can be shown that these surfaces of sections are transversal to the flow. As mentioned earlier, there exists an integral of motion in the model that allows us to reduce the dimensionality of the map by an additional dimension. The Poincaré map is computed at a given value of the Jacobi integral J, which makes this map a function of J.

In the three-dimensional case the resulting Poincaré map is four-dimensional, which means that we need four parameters to parametrize Σ_1 and Σ_2. On Σ_1 we consider the (y, z) coordinates in the plane $x = x_{L_2}$ plus two angles (δ, ϕ) for the direction of the velocity vector, whose magnitude v is determined by the Jacobi constant. With this parameterization the inital conditions on Σ_1 can be written as

$$x_0 = x_{L_2}, \qquad \dot{x}_0 = v\cos\phi\cos\delta \tag{16}$$

$$y_0 = y, \qquad \dot{y}_0 = v\cos\phi\sin\delta \tag{17}$$

$$z_0 = z, \qquad \dot{z}_0 = v\sin\phi \tag{18}$$

where $v = \sqrt{[2(J + 1/r) + (3x^2 - z^2)]}$ and δ, ϕ range in the interval $(-\pi/2, \pi/2)$.

On Σ_2 we use three spatial coordinates (x, y, z) or (r_p, ω, Ω), the periapsis radius, argument of periapsis, and longitude of the ascending node (relative to the positive x axis of the rotating frame), plus the inclination. This is merely a convenient way to obtain practical numerical conditions on escape.

Note that in the planar case, the Poincaré map requires only two parameters on Σ_1 and Σ_2. We choose y and δ on Σ_1 and (x, y) (or equivalently $(r_p, \tilde{\omega})$, periapsis radius and longitude of periapsis) on Σ_2. Figure 2 shows the geometry of the Poincaré maps considered in the planar case.

Given the initial conditions (16), (17), and (18), a 8(7) order Runge–Kutta–Fehlberg integration routine is used to integrate the trajectories backward to Σ_2. The initial points are chosen randomly on Σ_1. Symmetry S_3 is used to restrict the computation to the points $z > 0$, the symmetric points being obtained by directly applying the symmetry at periapsis. The Poincaré maps have been computed with at least 100×100 points in the planar case and 300×300 points in the three-dimensional case. The values of J vary from $J_{L_2} + 10^{-9}$ to $J_{L_2} + 0.11$. Examples of Poincaré maps at several Jacobi constant value are given in Fig. 3.

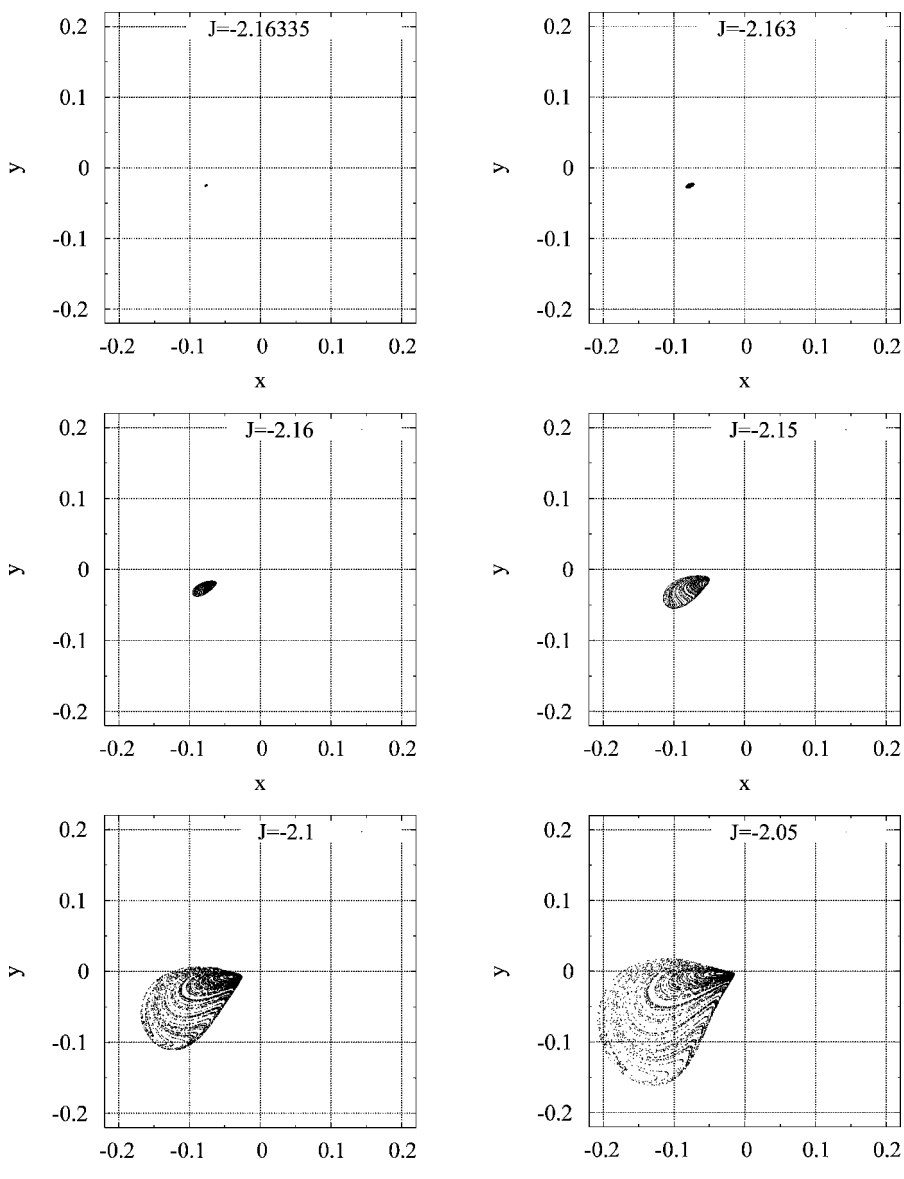

Fig. 3 Series of Poincaré maps (Σ_2^a) at several values of the Jacobi constant.

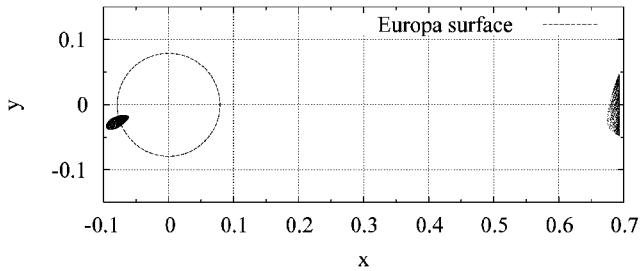

Full results

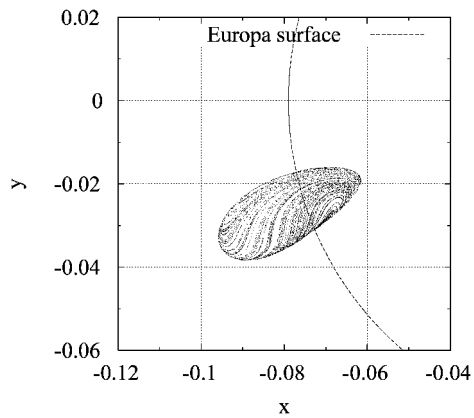

Close up near the satellite (Σ_2^a)

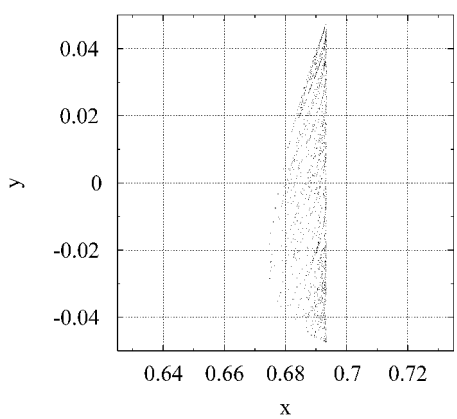

Close up near L_2 (Σ_2^b)

Fig. 4 Example of a two-dimensional Poincaré map for $J = -2.16$.

Results

Figure 4 gives an example of a Poincaré map for $J = -2.16$, together with two close-ups. As appears immediately on these figures, the image of the Poincaré map is divided into two (numerically) disjoint sets denoted Σ_2^a and Σ_2^b. The first one, Σ_2^a, is oval shaped and is close to the primary and confined to a small region of altitude and longitude of periapsis. It corresponds to trajectories that come from the neighborhood of the primary. The second set, Σ_2^b, is confined close to L_2 and corresponds to trajectories coming from the exterior region before exiting again.

When projected onto position space, the full four-dimensional Poincaré map has the same characteristic features as in the planar case. It is divided into two disjoints sets Σ_2^a and Σ_2^b, whose intersections with the (x, y) plane match the image of the Poincaré map in the planar case. The three-dimensional picture of Σ_2^a looks like the set of points obtained from the planar Σ_2^a by rotating it along its diameter (the line connecting the points of extremal radius on this set). Restrictions on inclination for Σ_2^a are given in Fig. 5. It can be checked that the extrema of the radius of the points in Σ_2^a are reached at some points in the (x, y) plane. The maximum of inclination is also reached at a point in the equatorial plane with $r < r_{L_2}$ (periapsis radius of the stable manifold associated with L_2). Σ_2^b fills the opening of the zero velocity surfaces, similar to the planar case.

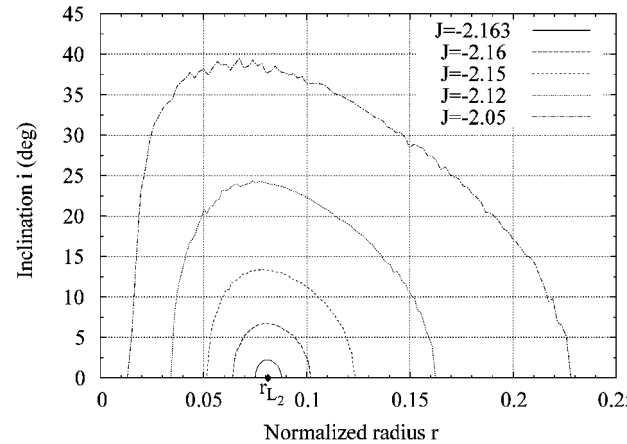

Fig. 5 Envelopes of the projections of a few Poincaré maps (Σ_2^a) onto the (r, i) space.

From a practical point of view, we will focus almost exclusively on the first region, Σ_2^a, in the remainder of our investigation. It is, indeed, the most important set to be considered for the practical application of these computations to the problem of direct escape from a planetary satellite.

Figure 3 shows a series of Poincaré maps at different values of Jacobi constant. It immediately appears on these figures that the set of points defining the Poincaré map enlarges as the Jacobi constant increases from J_{L_2}. At the limit, when $J \simeq J_{L_2}$, the Poincaré map reduces to a point that corresponds to the first periapsis of the stable manifold associated with L_2. Formally, this allows us to classify all of the planetary satellites according to whether or not this periapsis is above or below their physical surface. Miranda is of type 1 (periapsis below the surface); Europa, Titan, and Triton are of type 2 (periapsis above the surface). Note, however, that Europa is rather exceptional: the periapsis of the stable (and unstable) manifold associated with L_2 (or L_1) lies only 40 km above the surface of Europa. (Periapsis radius of the stable manifold $r_{L_2} \simeq 0.081$. Normalized radius of Europa $\simeq 0.079$.) We see that for type 1 satellites, it is possible to directly escape the surface of the body at the minimal energy necessary to escape, J_{L_2}, by performing an impulsive thrust at the surface, whereas for type 2 satellites one needs to go to higher energies to escape directly (see also the Optimal Transfers section). This classification also has some consequences for the capture problem, as is discussed later.

As just noted, as J varies the characteristics of the Poincaré maps vary. Some of these variations are captured in Figs. 6 and 7, which show the extrema of radius, longitude of the ascending node (or longitude of periapsis in two dimensions), eccentricity, and inclination as a function of J. Note that all of these extrema are reached at points in the equatorial plane. In particular, at these extrema $\omega = 0$ deg.

All of these graphs show that the set of first periapsis before escape Σ_2^a is confined in a rather narrow region even for large values of J. At $J = -2.05$ the opening at L_2 is four to five times the radius of Europa, whereas Σ_2^a extends over less than three radii.

As noticed earlier, by applying the symmetries S_4 and S_5 the preceding results apply for escape through L_1. That is, by taking the symmetry with respect to the origin (in phase space) of the set of points defining the Poincaré maps for L_2 we obtain the Poincaré maps relative to L_1. As concerns the characteristic properties of these maps, only the condition on Ω and $\tilde{\omega}$ are changed by a shift of 180 deg.

Similarly, applying S_1 and S_2 we obtain the Poincaré maps relative to the capture problem. Again, nothing changes in the curves given in Figs. 6 and 7, except that Ω transforms to $-\Omega$ and $\tilde{\omega}$ transforms to 180 deg $-\tilde{\omega}$. Here the type of the satellite determines the properties of capture of low energy particles. Type 1 satellites have a large set of trajectories coming from the exterior region that directly impact the surface of the satellite for values of J close to the critical value J_{L_2}. In fact, all transit trajectories[1] will ultimaltely impact the planetary satellite, so that there is no possibility of very low energy transit in these cases. On the contrary, type 2 satellites capture low-energy particles for at least one periapsis without impact. Further backward

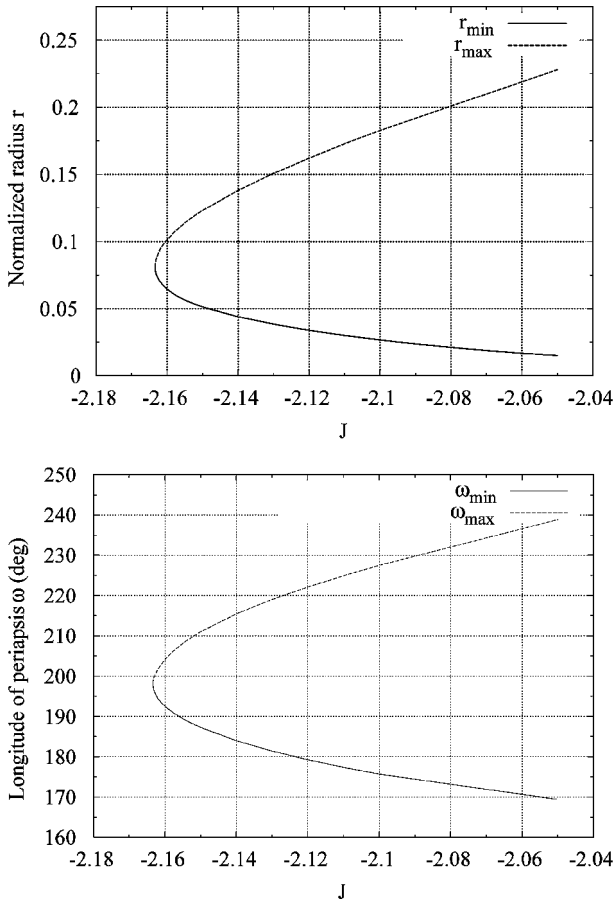

Fig. 6 Extrema of radius and longitude of periapsis on Σ_2^a as a function of J.

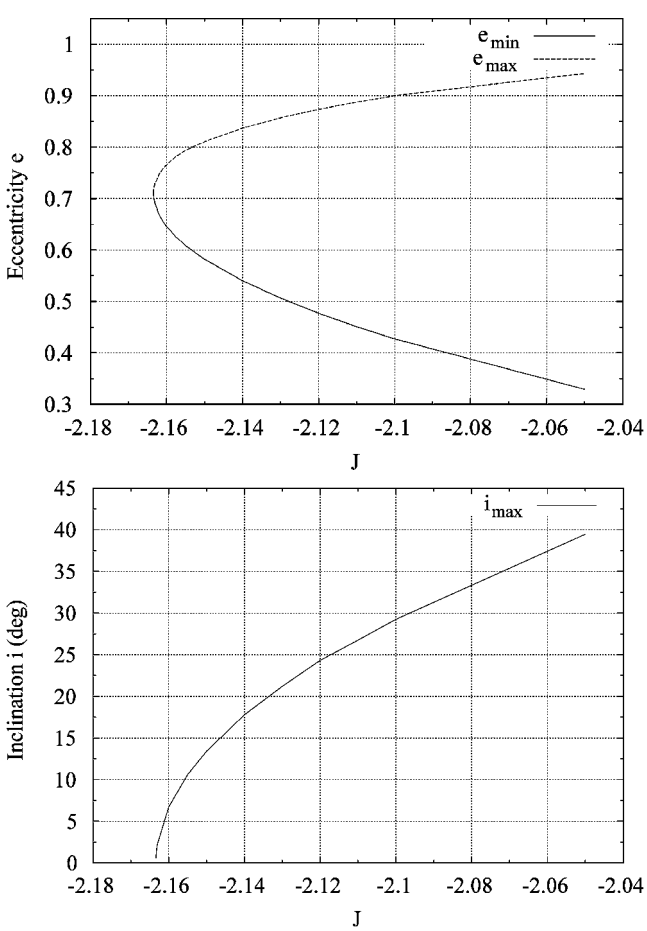

Fig. 7 Extrema of eccentricity and inclination on Σ_2^a as a function of J.

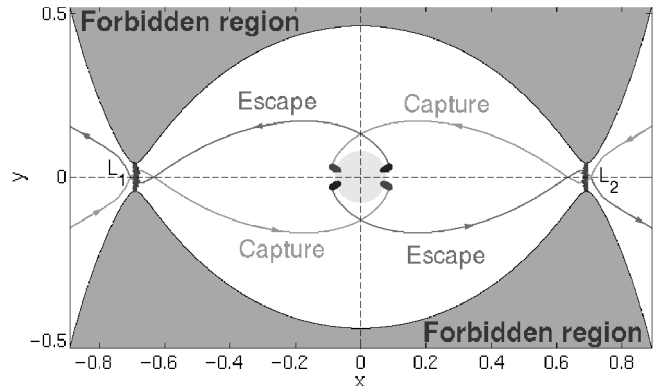

Fig. 8 Poincaré maps for escape and capture (case of Europa $J = -2.16$).

integration indicates that there is no impact for at least the first three periapsis if J is close enough to J_{L_2}. In the case of Europa, a low-energy particle might or might not directly impact the surface. Figure 8 gives a representation of the different Poincaré maps at $J = -2.16$ in the planar case for Europa.

Optimal Transfers

As mentioned in the Introduction, for low altitudes and inclinations ($r \leq 0.215$ and $i \leq 39.23$ deg) nearly circular orbits present a small periodic variation in eccentricity.[7] Therefore, under these conditions we can approximate the motion of a spacecraft by a uniform circular motion and consider what minimum ΔV is needed to escape such a planetary satellite starting in a low-altitude, circular orbit (or equivalently, be captured into a low-altitude, circular orbit).

This question can be viewed from two different points of view. The first one asks if there is a particular altitude for which the ΔV to escape is minimal among all direct escape maneuvers starting in low-altitude circular orbits. The second assumes the spacecraft is in a low-altitude circular orbit and asks what the minimal ΔV to escape from this given orbit is. With this last problem one must investigate all of the possible techniques to escape starting in a low-altitude, circular orbit to obtain an optimal escape criterion. The first problem is then answered as a consequence of this criterion and the method used to derive it.

After proving that tangential burns are optimal for escape maneuvers, different strategies for performing the maneuver are evaluated, leading to an optimal criterion in the planar case. Then, the three-dimensional case is considered. All of this analysis uses the computations explained in the preceding section.

Planar Case

Tangential Burns Are Optimal

When in a circular orbit, the ΔV needed to place a spacecraft into an arbitrary trajectory crossing the circular orbit can be expressed as

$$\Delta V = |\boldsymbol{v} - \boldsymbol{v}_{\mathrm{lc}}| = \sqrt{v^2 + v_{\mathrm{lc}}^2 - 2 v v_{\mathrm{lc}} \cos\gamma} \tag{19}$$

where $v_{\mathrm{lc}} = \sqrt{(1/r) - r}$ is the local circular speed at a given radius r expressed in the rotating frame, $v = \sqrt{[2(J + 1/r) + 3x^2]}$ is the speed of the arbitrary trajectory, and γ is the flight-path angle. [$v_{\mathrm{lc}} = \sqrt{[1/r - (x^2 + y^2) - 2\sqrt{r}\cos i]}$ in three dimensions.]

From these expressions it is clear that v and ΔV (parameterized by the Jacobi constant J) increase with J, so that we first look at the minimum value of ΔV for $J = J_{L_2}$. This means that at each point of the stable manifold associated with L_2 we must compare $\boldsymbol{v}$ to the local circular velocity and look for the minimum of ΔV.

This can be done numerically, and it appears that $\Delta V \geq 1$, at least up to the apoapsis following the first periapsis passage (in backward integration), with a minimum at periapsis and a rather strong increase around it. This fact can also be justified analytically, the result holding for any values of $J \leq 0$ (under some weak restrictions on radius and eccentricity at periapsis). This shows that the minimum ΔV is obtained for tangential burns (i.e., at periapsis), and these maneuvers are hence more optimal than an arbitrary nontangential maneuver. This fact justifies a posteriori the use of

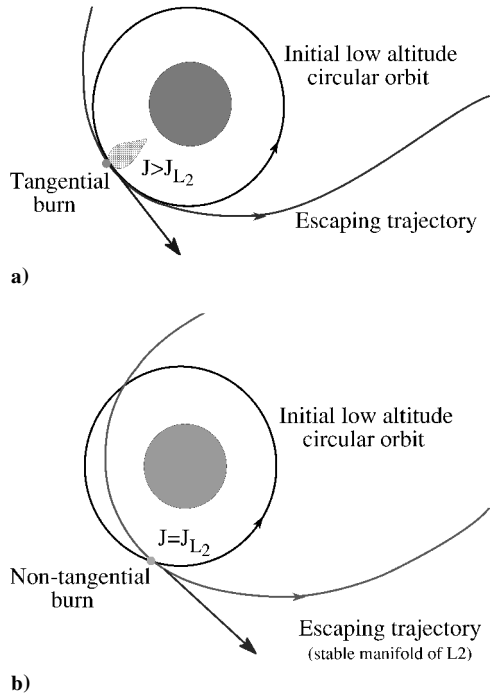

Fig. 9 Strategies to escape: a) first strategy: increase J and perform a tangential burn and b) second strategy: nontangential burn to place the spacecraft into the stable manifold associated with L_1 or L_2.

the Poincaré maps considered in the preceding section to obtain practical optimal criterion for escape.

It seems, at this point, that the optimal value of r, which minimizes ΔV would be the periapsis of the stable manifold associated with L_2, but the following sections show how to choose better values.

Strategies to Escape

In the preceding section we showed that along an escaping trajectory the minimum ΔV to escape is reached at periapsis with a tangential burn. Because $\partial \Delta V / \partial J = 1/v > 0$, it also shows that this ΔV is the true optimal value if the altitude of the inital circular orbit is exactly equal to the periapsis radius r_{L_2} of the stable manifold of L_2. However, for arbitrary r this case is not met in general. Two strategies for escape are then possible. The first one consists of considering a larger value of J so that the Poincaré map reaches the given radius [i.e., $r \in \Sigma_2^a(J > J_{L_2})$]. Then, a tangential burn is applied at the periapsis of an escaping trajectory. We indeed saw in the subsection Results that the range of altitudes reached by Σ_2^a increases as J increases. The second strategy, only applicable for $r \geq r_{L_2}$, consists of performing a nontangential burn to place the spacecraft on the stable manifold of L_2. For $r < r_{L_2}$ only the first strategy is applicable in the case of single-impulse, direct-escape maneuvers. Figure 9 illustrates the geometry of these two strategies.

Let us for now assume $r > r_{L_2}$ and compare these strategies. To do so, we compute the minimum ΔV possible using the first strategy, the ΔV corresponding to the second approach being greater than or equal to one.

Minimum ΔV as a Function of J

For $J > J_{L_2}$, Σ_2^a is not reduced to a single point, and on this set ΔV is a function of radius r and longitude of periapsis $\tilde{\omega}$. We can show that for $r < 0.35$ and $J < -1$, $\partial \Delta V / \partial r < 0$ and the minimum ΔV is reached on the boundary of the Poincaré map at a point close to (but not equal to) the maximal radius point in the Poincaré map. Denoting $\Delta V_{\min}(J)$ this minimal value at a given J, we can numerically compute this value at several values of the Jacobi constant. The altitude r at which $\Delta V_{\min}$ is reached increases with J so that we can also compute $\Delta V_{\min}(r)$, which is more convenient from a practical point of view. Figure 10 gives the results of such a computation.

We clearly see that $\Delta V_{\min}$ decreases as a function of r. This result allows us to choose the first strategy as being optimal. Indeed, for $J_0 > J_{L_2}$, $\Delta V_{\min} \leq \Delta V(r, \tilde{\omega}, J_0)$, where $(r, \tilde{\omega}) \in \Sigma_2^a(J_0)$.

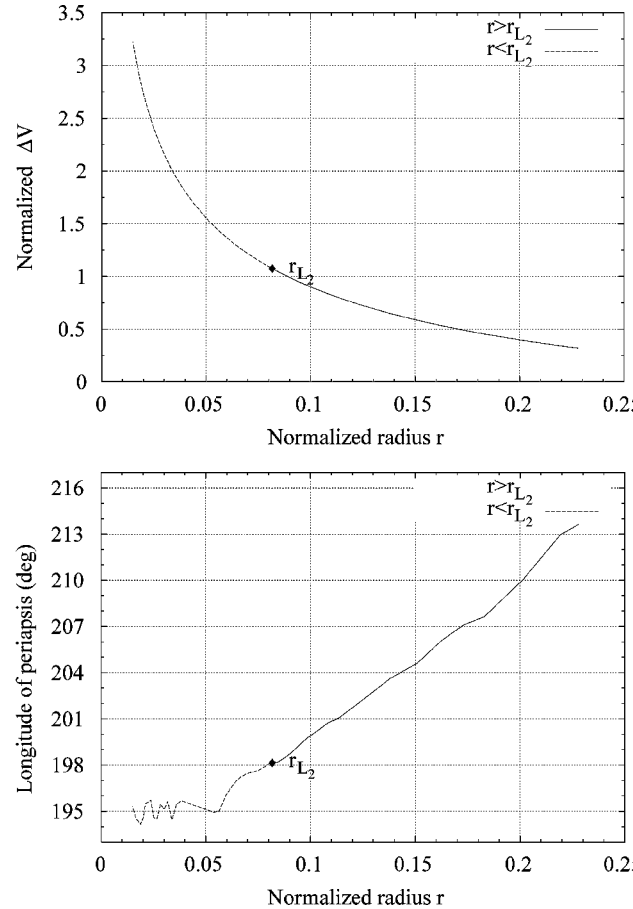

Fig. 10 Optimal ΔV and longitude of periapsis for escape.

Now $\Delta V(r, \tilde{\omega}, J_0) \leq \Delta V_{\text{traj}}(r, \tilde{\omega}, J_0)$, where ΔV_{traj} corresponds to the ΔV calculated at any point of an escape trajectory having $(r, \tilde{\omega}, J_0)$ as periapsis (by the optimality of tangential burns). Therefore, $\Delta V_{\min}(J_0) \leq \Delta V_{\text{traj}}(r, \tilde{\omega}, J_0)$ for any $r, \tilde{\omega}$ in the Poincaré map at a given Jacobi constant J. By the fact that $\Delta V_{\min}$ decreases as J increases, we see that this inequality is, in fact, satisfied for any $(r, \tilde{\omega}) \in \Sigma_2^a(J \leq J_0)$. In particular, $\Delta V_{\min}(J_0) \leq \Delta V_{\text{traj}}(J_{L_2})$, that is, the first startegy for escape is more optimal than the second strategy.

For $J \geq J_0$ no optimality of $\Delta V_{\min}(J_0)$ has been proven. {That is, it may happen that $\Delta V[J, r, \tilde{\omega}(J)]$ (as taken on the boundary of Σ_2^a) is slightly less than $\Delta V_{\min}[J_0, r, \tilde{\omega}(J_0)]$ for J slightly greater than J_0. Settling this question depends on evaluating $\partial \tilde{\omega} / \partial J$ at a fixed r on the boundary of Σ_2^a, which is a difficult quantity to compute.} However, from a practical point of view it can be shown that the value $\Delta V_{\min}$ is very close to the true optimum (see subsection Nonplanar Case).

Optimal Criterion

For $r < r_{L_2}$ the strategy to escape is similar to the case $r \geq r_{L_2}$. However, in this case the minimum ΔV to escape does not correspond to the minimum ΔV taken over the set Σ_2^a. It is reached at a point near (but not exactly at) $r_{\min}$. From a practical point of view, $r_{\min}$ is considered as an optimal solution in this case.

When applying a tangential burn at a given point, the elements of the transfer trajectory are fixed at periapsis. Therefore, at the time of the maneuver $\tilde{\omega}$ is equal to the polar angle (which is approximated by Nt in a circular orbit), which allows us to characterize the placement of the maneuver in terms of $\tilde{\omega}$. Using this remark and the results of the preceding sections, we obtain the following escape criterion: *Starting in a low-altitude, circular orbit at a given radius r fuel optimal direct-escape maneuvers are obtained using an impulsive thrust, tangential to the path, whose magnitude and placement are determined, respectively, by $\Delta V(r)$ and $\tilde{\omega}(r)$, as given in Fig. 10.* (Because of the discrete nature of the calculations and the rather sharp edge of the Poincaré map at $r_{\min}$, the results for the longitude of periapsis for $r < r_{L_2}$ cannot be considered very accurate for

Table 2 Minimum ΔV to escape the surface of some planetary satellites

Planet		Satellite	Nondimensional ΔV	ΔV scale factor, m/s	ΔV to escape, m/s	Keplerian ΔV to escape, m/s	Savings when comp. to Kepler, m/s
Earth		Moon	2.79	235.4	656.8	695.7	38.9
Mars	II	Deimos	0.44	1.9	0.8	1.9	1.1
Jupiter	I	Io	0.76	624.7	474.8	748.7	273.9
	II	Europa	1.12	402.9	451.2	590.9	139.7
	III	Ganymede	1.44	464.9	669.5	802.8	133.3
	IV	Callisto	2.04	315.0	642.6	716.0	73.4
	X	Lysithea	2.75	1.1	3.0	3.3	0.3
Saturn	II	Enceladus	0.38	64.0	24.3	58.2	33.9
	III	Thethys	0.52	123.8	64.4	126.3	61.9
	IV	Dione	0.75	123.1	92.3	146.6	54.3
	V	Rhea	1.00	139.0	139.0	193.5	54.5
	VI	Titan	2.02	345.3	697.5	775.6	78.13
	VII	Hyperion	2.08	15.7	32.7	36.3	3.6
Uranus	I	Ariel	0.75	137.5	103.1	163.5	60.4
	II	Umbriel	0.96	111.0	106.6	151.1	44.5
	III	Titania	1.53	125.2	191.6	225.8	34.2
	IV	Oberon	1.92	102.7	197.2	212.5	15.3
	V	Miranda	0.37	62.0	22.9	57.5	34.6
Neptune	I	Triton	1.42	260.8	370.3	426.3	56.0
Pluto	I	Charon	1.58	135.8	214.6	252.4	37.8

large values of J. This appears clearly on this plot, even though the computations have been done with 300×300 points in this case.)

Note that this optimal escape criterion is sufficient and necessary (with the definition of escape adopted in this paper). In particular, escape is always achieved for a tangential $\Delta V > \Delta V_{\text{opt}}$. Indeed, this condition implies that $J > J_{\text{opt}}$ and $\Sigma_2^a(J) \supset \Sigma_2^a(J_{\text{opt}})$. The optimal point at Jacobi constant J_{opt} hence lies inside $\Sigma_2^a(J)$ and is still the periapsis of an escape trajectory.

This last result can prove useful for applications because it leads to stability of escape relative to errors in the initial thrust. In fact, because the optimal point is not isolated small errors in thrust direction correspond to placing the spacecraft on an escaping trajectory with periapsis near the optimal value. That is, escape maneuvers are also robust to small errors in thrust direction.

Note, however, that, as stated in the Introduction, these results only consider escape from the Hill region and are not concerned with the long-term behavior of the trajectories. Small corrections near L_1 or L_2 might be necessary to avoid capture in the future. This long-term analysis should be performed using a model that describes the dynamics of the secondary like the CR3BP and might be more dependant on the particular planetary-satellite system considered.

Finally, besides quantitatively determining fuel-optimal direct-escape maneuvers, Fig. 10 shows that the answer to the first initial question is negative: there is no optimal value of r such that ΔV is minimal among all directly escaping transfers for low circular orbits ($r < 0.23$). Even if such a minimum exists for larger r, the assumption for a spacecraft to be in a circular orbit at this radius is not valid anymore and the definition of ΔV is less meaningful.

Applying our preceding results to the available planetary satellites (whose normalized radius are covered by the range of Jacobi constant considered), we can compute the minimal ΔV to escape from these planetary satellites starting in a circular orbit at a low altitude ($h \simeq 0$). The savings compared to a Keplerian escape maneuver (parabolic trajectory) are also computed and summarized in Table 2. Note that savings on the order of 130 m/s in the case of Europa are obtained.

Nonplanar Case

As noticed in subsection Results, the extrema of r and i over Σ_2^a are reached at some point in the equatorial plane ($z = 0$). This is also true for ΔV, for which the minimal value is reached at $r \simeq r_{\max}$. The earlier optimal criterion is therefore still valid in three-dimensional space. However, in this case one can ask what is the minimum ΔV to escape starting in a nonzero inclination initial orbit.

Variations in Inclination

As J varies, the ranges of inclination reached by the Poincaré maps increase, reaching rather large values for relatively large values of J (see Fig. 7).

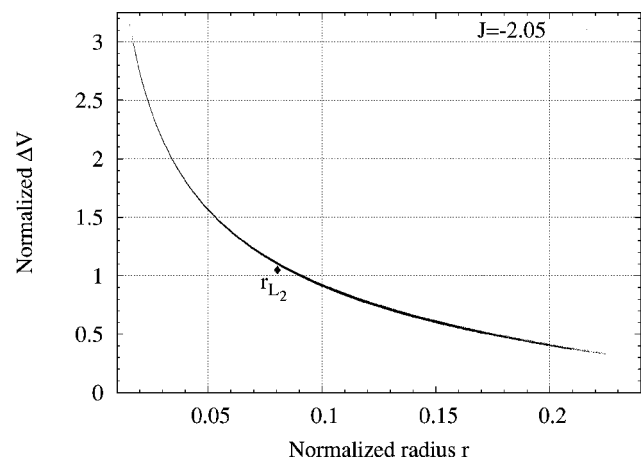

Fig. 11 Projection of a Poincaré map onto the $(r, \Delta V)$ space.

The radius where the maximal inclination is reached decreases with J. However, it is still true that at any fixed r the maximum in inclination increases with J. Figure 5 gives the envelope curve of a series of Poincaré maps at several values of Jacobi constant, projected onto the (r, i) space.

Strategy to Escape Starting in a Nonzero Inclined Orbit

Even though the optimality of tangential burns has only been considered in the planar case so far, the demonstration in three-dimensional space follows the same line. That is, it is still true that tangential maneuvers are optimal when compared to nontangential ones. This leads us to choose the same approach to the problem as in the planar case (see subsection Strategies to Escape).

Starting from a nonzero inclination, low-altitude, circular orbit (determined by the radius r and the inclination i), the strategy to escape consists of increasing J so that the maximal inclination reached by the Poincaré map at the given radius r equals the initial inclination i. Then, a tangential maneuver is applied at this point of maximal inclination (at fixed radius r). Because we know that this maximum is reached in the equatorial plane ($z = 0$), we have the condition $\omega = 0$ deg at the time of the maneuver. The longitude of the ascending node at such point is restricted to lie in the range $[\Omega_{\min}, \Omega_{\max}]$, as determined by Fig. 6.

Next arises the question of the optimality of such an approach, for which no definite result is given in this paper. However, a hint at the near optimality of such an approach is given in Fig. 11, which presents the projection of a Poincaré maps onto the $(r, \Delta V)$ space. We can see on this graph that at any fixed radius r and Jacobi constant J the variations of ΔV over the cross section of the Poincaré map

are very small (less than 0.05). In fact, as J decreases the thickness of the cross sections decreases as well, so that for all of the values of J considered in this paper the variations of ΔV over a Poincaré map at a fixed radius r are less than 0.05. Moreover, because, as J increases, ΔV increases at any fixed point, it can be concluded that, in the case of nonoptimality of the preceding approach, the value obtained is very close to the true optimum.

Operation of the Maneuver

The preceding discussion proved the existence of an optimal ΔV to escape starting at an inclination i. This ΔV is well approximated by the values given in Fig. 11, and this might be sufficient from a practical point of view (less than 5% error on the total ΔV costs in the case of Europa as a result of the small variations of ΔV across Σ_2^a at fixed radius r). We also saw that this optimum is reached for $\omega = 0$ deg, even though no precise condition has been given for Ω, but for the bounds given in Fig. 6.

From a theoretical point of view, we know, however, that whatever the optimal value for Ω is, it can be targeted with an arbitrary precision by correctly choosing the time of the maneuver. Indeed, the position of the spacecraft at the time of the maneuver fixes ω and Ω at the periapsis of the escape trajectory. Therefore, at any given time we can associate the position of the spacecraft in its inital orbit with some values of ω and Ω that would correspond to the values taken if the maneuver were actually performed at that time. We hence obtain two functions of time $\omega(t)$ and $\Omega(t)$. Because the initial orbit is assumed circular and the frame is rotating, the point $[\omega(t), \Omega(t)]$ draws a line on the torus space $[0, 2\pi]^2$, which indicates that any value of ω and Ω can be reached to arbitrary precision by waiting for a sufficiently long time {assuming that the slope of the line $[\omega(t), \Omega(t)]$ is irrational}.

Conclusions

Escaping and capture trajectories in the Hill three-body problem have been investigated using a Poincaré map. This map allowed us to characterize the set of periapses before escape (or after capture) by some bounds on radius, longitude of periapsis, and inclination. These results have been applied to the problem of determining the minimum ΔV needed to escape from a planetary satellite, starting in a low-altitude, circular orbit. An optimal criterion has been given in the planar case, and a practical approach has been given in the three-dimensional case. It is shown that the resulting cost for escape decreases as the initial altitude increases. The cost to escape in the vicinity of a planetary satellite is on the order of the ΔV scale factor $(\mu N)^{1/3}$ and represents significant savings as compared to a parabolic escape. Future work will try to characterize more fully the optimality in the three-dimensional case, study the separation of the image of the Poincaré map into two disjoints sets, and analyze the Poincaré maps between previous periapsis passages.

Appendix: Scaling of the Results to Planetary Satellites

Tables 1 and 2 apply the results found in the paper to all of the planetary satellites in the solar system whose mass, orbital period, and radius are known.[11] Further restrictions apply for the scaling of the ΔV needed to escape: because of the range of Jacobi constant considered, the normalized radius must be greater than 0.08 and less than 0.23 (Table 2).

In Table 1, $l = (\mu/N^2)^{1/3}$ and $\tau = 1/N$ are the unit length and timescale used to normalize the Hill equations (see subsection Normalization and Scaling to Any Planetary Satellite). The type has been defined in the subsection Results. In Table 2 the nondimensional ΔV is read from Fig. 10 (r being, in this case, the normalized radius of the planetary satellite). The ΔV scale factor is given by $(\mu N)^{1/3}$, and the Keplerian ΔV to escape is $\sqrt{(\mu/r)}(\sqrt{2}-1)$. All of the ΔV values can be interpreted either as representing values in inertial space or in the rotating frame, as the correction caused by the rotation cancels out when computing differences in velocities at the same position.

Acknowledgment

The work described was funded by the TMOD Technology Program and Outer Planets/Solar Probe Project by grants from the Jet Propulsion Laboratory, California Institute of Technology, which is under contract with NASA.

References

[1] Conley, C. C., "Low Energy Transit Orbits in the Restricted Three-Body Problem," *SIAM Journal of Applied Mathematics*, Vol. 16, No. 4, 1968, pp. 732–746.

[2] Belbruno, E. A., "Sun-Perturbed Earth-to-Moon Transfers with Ballistic Capture," *Journal of Guidance, Control, and Dynamics*, Vol. 16, No. 4, 1993, pp. 770–775.

[3] Koon, W. S., Lo, M. W., Marsden, J. E., and Ross, S. D., "Heteroclinc Connections Between Periodic Orbits and Resonance Transitions in Celestial Mechanics," *Chaos*, Vol. 10, No. 2, 2000, pp. 427–469.

[4] Koon, W. S., Lo, M. W., Marsden, J. E., and Ross, S. D., "Low Energy Transfer to the Moon," *Celestial Mechanics and Dynamical Astronomy*, Vol. 81, No. 1, 2001, pp. 63–73.

[5] Hénon, M., and Petit, J. M., "Series Expansions for Encounter-Type Solutions of Hill's Problem," *Celestial Mechanics and Dynamical Astronomy*, Vol. 38, No. 1, 1986, pp. 67–100.

[6] Hill, G. W., "Researches in the Lunar Theory," *American Journal of Mathematics*, Vol. 1, No. 1, 1878, pp. 5–26.

[7] Scheeres, D. J., Guman, M. D., and Villac, B. F., "Stability Analysis of Planetary Satellite Orbiters: Application to the Europa Orbiter," *Journal of Guidance, Control, and Dynamics*, Vol. 24, No. 4, 2001, pp. 778–787.

[8] Hénon, M., "Numerical Exploration of the Restricted Problem.V. Hill's Case: Periodic Orbits and Their Stability," *Astronomy and Astrophysics*, Vol. 1, No. 2, 1969, pp. 223–238.

[9] Montenbruck, O., and Gill, E., *Satellite Orbits: Models, Methods, and Applications*, Springer-Verlag, Berlin, 2000, p. 55.

[10] Arnol'd, V. I., *Dynamical Systems III, Encyclopedia of Mathematical Sciences*, Springer-Verlag, Berlin, 1988, pp. 72–75.

[11] Seidelmann, Kenneth P., *Explanatory Supplement of the Astronomical Almanac*, Univ. Science Books, Mill Valley, CA, 1992, pp. 708–711.

[12] Wiggins, S., *Introduction to Applied Nonlinear Dynamical Systems and Chaos*, Springer-Verlag, New York, 1990, pp. 64–192.